Tandem Repeat-Like Domain of "Similar to Prion Protein" (StPrP) of Japanese Pufferfish Binds Cu(II) as Effectively as the Mammalian Protein†

Paweł Stanczak,‡ Daniela Valensin,§ Elena Porciatti,§ Elzbieta Jankowska,⊥ Zbigniew Grzonka,⊥ Elena Molteni,§ Elena Gaggelli,§ Gianni Valensin,*,§ and Henryk Kozlowski*,‡

Faculty of Chemistry, University of Wrocław, F. Joliot-Curie 14, 50-383 Wroclaw, Poland, Department of Chemistry, University of Siena, via Aldo Moro, 53100 Siena, Italy, and Faculty of Chemistry, University of Gdansk, Gdansk, Poland

Received June 6, 2006; Revised Manuscript Received July 24, 2006

ABSTRACT: The main structural domains of prion proteins, in particular the N-terminal region containing characteristic amino acid repeats, are well conserved among different species, despite divergence in primary sequence. The repeat region seems to play an important role, as verified by pathogenicity only observed in organisms having repeats composed of eight residues. In this work three different peptides belonging to the tandem repeat region of StPrP-2 from the Japanese pufferfish *Takifugu rubripes* have been considered; the coordination modes and conformations of their complexes with Cu(II) have been investigated by using potentiometric titrations, spectroscopic data, and restrained molecular dynamics simulations. In all cases the histidine imidazole(s) provide the anchoring site for copper, with the further involvement of amide nitrogens depending on the peptide sequence and on pH. An increase in copper binding affinity has been observed going from the shortest peptide, corresponding to a single repeat and containing two histidines, to the longest one, encompassing three repeats with six histidines.

The prion protein (PrP), a ubiquitous protein most prominently expressed in the brain (*1*), is the object of intensive investigations because of the widespread occurrence of transmissible spongiform encephalopathy (TSE).[1] The normal cellular isoform (PrP^C) is involved in replicating the causative agent, which, according to the prion hypothesis, is a misfolded or scrapie prion isoform (PrP^{Sc}) (*1*). The physiological role of PrP^C is still largely unclear; however, the protein is well-known to bind copper in vivo, and its superoxide dismutase activity has been reported, possibly indicating a neuroprotective role against oxidative stress (*2*).

Transmission of TSE between species depends on the degree of sequence similarity at the specific amino acids involved in the interaction between the infectious PrP^{Sc} and the host's PrP^C molecules (*3*, *4*). Variability at these sites can create "host barriers" (*4*−*6*), although infection between distant species can also occur after long exposure times (*3*).

Despite divergence in primary sequence, the main structural domains of prion proteins are well conserved among different species (*7*−*10*), and they can therefore be easily compared in order to reveal functional evolutionary trends possibly related to aspects of prion pathogenesis. In particular, the N-terminal domain contains, within each vertebrate class, a distinctive number of degenerate amino acid repeats. The repeat units have increased their length going from fish to human, reaching a maximum of eight amino acids in mammals. Interestingly, scrapie pathogenicity, related to the self-aggregating properties of the prion protein, has been observed only in mammals, i.e., only in the case of PrPs having octarepeats (*11 and refs therein*).

Recently, cDNAs have been identified in Japanese pufferfish (*Takifugu rubripes*) coding homologues to tetrapod prion protein (PrPs) termed "similar to PrP", StPrP-1 and StPrP-2 (*12*). The 450 residues StPrP-1 possesses all features common with the family of PrP, namely, a signal sequence, two lysine clusters, a Gly-Pro-rich domain, a hydrophobic region, two cysteine residues potentially involved in the formation of an intramolecular disulfide bond, a glycosylation site, and a presumable GPI-anchor site. In addition, StPrP-1 is a relatively basic protein with pI = 9.57 similar to that of tetrapod PrP (*12*−*14*). The StPrP-2 cDNA codes for a 425 residues protein with pI = 9.14, which, similarly to StPrP-1, exhibits common features to tetrapod PrP including signal sequence, two typically positioned cysteine residues, potential glycosylation sites, supposed GPI anchor, and a Gly-Pro-rich region (*8*). Such similarities are expected to yield elements of secondary and tertiary structure of StPrP-2 closely related to the known PrP fold, with the Gly-Pro-rich

† This work was supported by the Polish Ministry of Education and Science (MEiN 1 T09A 149 30, DS/8350-4-0131-6), and by the MIUR FIRB RBNE03PX83_003. We acknowledge the CIRMMP (Consorzio Interuniversitario Risonanze Magnetiche di Metalloproteine Paramagnetiche) for financial support.

* To whom correspondence should be addressed. Phone: +39-0577-234231 (G.V.); +48-71-3757251 (H.K.). Fax: +39-0577-234254 (G.V.); +48-71-3757251 (H.K.). E-mail: valensin@unisi.it (G.V.); henrykoz@wchuwr.chem.uni.wroc.pl (H.K.).

‡ University of Wrocław.

§ University of Siena.

⊥ University of Gdansk.

[1] Abbreviations: NMR, nuclear magnetic resonance; CD, circular dichroism; EPR, electronic paramagnetic resonance; PrP^C, cellular prion protein; PrP^{SC}, scrapie prion protein; TSEs, transmissible spongiform encephalopathies; StPrP, similar to prion protein; TOCSY, total correlation spectroscopy; ROESY, rotational nuclear Overhauser effect spectroscopy; NOESY, nuclear Overhauser enhancement spectroscopy; IR, inversion recovery; HSQC, heteronuclear single quantum correlation; HMBC, heteronuclear multiple bond correlation; MD, molecular dynamics; RMSD, root-mean-square deviation.

10.1021/bi061123k CCC: $33.50
Published on Web 09/19/2006

region forming an unstructured flexible domain as repeatedly found for all the investigated tandem repeat regions (*7*−*10*).

Studying prion proteins from different species is expected to provide valuable information on PrP molecular evolution as well as on structure/function relationships. In particular, copper binding to the N-terminal repeat regions of human (*15*−*17*) and chicken (*18*−*20*) PrP has been reported to occur in similar cooperative ways. It may therefore be rather important to investigate copper coordination properties of prion proteins from species phylogenetically far from each other.

In the present work, the structure and copper binding mode of three peptides derived from the tandem repeat region of StPrP-2 from the Japanese pufferfish *Takifugu rubripes* (*8*) have been investigated by potentiometric titrations, spectroscopic data including NMR, and restrained MD simulations. The considered peptides are (i) the $StPrP2_{96-104}$ fragment (Ac−GHGYGVYGH−NH_2 hereafter called fugu1), (ii) $StPrP2_{96-116}$ (Ac−GHGYGVYGH−PGYG−GHGYGVYG−NH_2, fugu2), two consecutive almost identical repeats lacking the last histidine, connected by the linker PGYG, and (iii) $StPrP2_{96-128}$(Ac−GHGYGVYGH−PGYG−GHGYGVYGH−PGYG−GHGFHGR−NH_2, fugu3), three consecutive repeats connected by PGYG linkers.

MATERIALS AND METHODS

Peptide Synthesis and Purification. Peptide synthesis was performed on a solid phase using Fmoc (Fmoc = 9-fluorenylmethoxycarbonyl) strategy with continuous-flow methodology (9050 Plus Millipore peptide synthesizer) on a polystyrene/poly(ethylene glycol) copolymer resin (TentaGel R RAM resin) (*21*).

Attachment of the first amino acid to the resin and next coupling steps were realized using diisopropylcarbodiimide (DIPCI) as a coupling reagent in the presence of 1-hydroxybenzotriazole (HOBt) in dimethylformamide (DMF)/*N*-methylpyrrolidone (NMP)/methylenechloride/Triton X-100 (33:33:33:1, v/v) mixture.

Removal of the Fmoc protecting group during peptide synthesis was achieved by action of 20% piperidine solution in DMF/NMP (1:1, v/v) with addition of 1% Triton X-100 (*22*). The N-terminal amino group was acetylated using 1 M acetylimidazole in DMF (*22*, *23*).

All peptides were cleaved from the resin and deprotected by treatment with the reagent B (88% trifluoroacetic acid, 5% phenol, 2% triisopropylsilane, 5% water) for 2 h at room temperature (*22*).

The resulting crude peptides were purified by reversed-phase high-performance liquid chromatography (RP-HPLC) using a C_8 semipreparative Kromasil column (25 mm × 250 mm, 7 μm). The purity of the peptides was confirmed by matrix-assisted laser desorption/ionization time-of-flight mass spectrometry (MALDI-TOF MS) and analytical RP-HPLC using a C_4 Kromasil column (4.6 mm × 250 mm, 5 μm) and a 30 min linear gradient of 0−80% acetonitrile in 0.1% aqueous trifluoroacetic acid as a mobile phase (Figure 1s).[2]

Analytical data were as follows: fugu1, R_t = 10.7 min, MS = 987.1 [M^+], calcd 987.1; fugu2, R_t = 13.0 min, MS = 2152.3 [M^+], calcd 2152.3; fugu3, R_t = 12.4 min, MS = 3411.9 [$M^+ - 1$], calcd 3412.7.

Potentiometric Measurements. Stability constants for both proton and Cu(II) complexes were calculated from three titrations carried out over the pH range of 3−11 at 298 K using a total volume of 3 mL. The purities and the exact concentration of the ligand solutions were determined by the method of Gran (*24*). NaOH was added from a 0.500 mL micrometer syringe which was calibrated by both weight titration and the titration of standard materials. The ligand concentration was 1 mM (for the fugu1 fragment) and 0.7 mM (for the fugu2 and fugu3 fragments). The metal-to-ligand molar ratio was 1:1. The pH metric titrations were performed at 298 K in 100 mM KNO_3 in water (for fugu1) or in 30:70 v/v DMSO/water (for fugu2 and fugu3) on a MOLSPIN pH meter system. A normal Russel CMAW 711 semicombined electrode was used, which was calibrated in proton concentrations with aqueous HNO_3 or HNO_3 dissolved in 30:70 v/v DMSO/water (*25*). The calculated ionic products for water and DMSO/water solutions were 13.770 and 14.523, respectively. The SUPERQUAD and HYPERQUAD 2000 programs were used for stability constant calculations (*26*, *27*). Standard deviations, as computed by SUPERQUAD and HYPERQUAD 2000, though referring to random errors only, provide a good indication of the importance of any particular species in the equilibrium.

EPR, UV−*Vis, and CD Measurements.* Similar concentrations as those used in potentiometric studies were employed; 30% ethylene glycol was used as a cryoprotectant for EPR measurements. Electron paramagnetic resonance (EPR) spectra were recorded on a Bruker ESP 300E spectrometer at X-band frequency (9.3 GHz) in liquid nitrogen. The EPR parameters were calculated from the spectra obtained at the maximum concentration of the particular species for which well-resolved separations were observed. The absorption spectra were recorded on a Beckman DU 650 spectrophotometer. Circular dichroism (CD) spectra were recorded on Jasco J 715 spectropolarimeter in the 750−240 nm range. The values of $\Delta\epsilon$ (i.e., ϵl − ϵr) and ϵ were calculated at the maximum concentration of the particular species obtained from the potentiometric data.

NMR Spectroscopy. The peptides were dissolved in water containing 10% deuterium oxide or in deuterium oxide. The pH was adjusted with either DCl or NaOD. The desired concentrations of metal ions were obtained by adding aliquots of stock aqueous solutions of $Cu(NO_3)_2$, and the pH was again checked and eventually readjusted. TSP-d_4, 3-trimethylsilyl-[2,2,3,3-d_4] propionate sodium salt, was used as the internal reference standard.

NMR measurements were performed at 14.1 T with a Bruker Avance 600 MHz spectrometer at controlled temperatures (± 0.2 K) using a TBI (triple broadband inverse) probe. Water suppression was achieved by the excitation sculpting method (*28*). A typical NMR spectrum required eight transients acquired with a 10 μs 90° pulse and 1.0 s recycling delay. Proton resonance assignment was accomplished through TOCSY, NOESY, and ROESY standard experiments. TOCSY spectra were obtained using the MLEV-17 pulse sequence with a mixing time of 75 ms. NOESY and ROESY spectra were obtained at different values of the mixing time to optimize the best one. Carbon resonance assignment was obtained through $^1H-^{13}C$ HMBC

[2] Figures and tables labeled with "s" can be found in the Supporting Information.

Table 1: Potentiometric and Spectroscopic Data for Proton and Cu^{2+} Complexes of Ac−GHGYGVYGH−NH_2[a]

			UV−vis		CD		EPR	
species	log β	log K	λ/nm	ϵ/M^{-1} cm^{-1}	λ/nm	$\Delta\epsilon$/M^{-1} cm^{-1}	$A_{\|}$/G	$g_{\|}$
fugu1								
HL	10.19(1)	log K_{Tyr} = 10.19						
H_2L	19.69(1)	log K_{Tyr} = 9.50						
H_3L	26.46(1)	log K_{im} = 6.77						
H_4L	32.50(1)	log K_{im} =6.04						
CuH_3L	29.91(2)		minor					
CuH_2L	25.36(3)	4.55	659	41	309	0.031	175	2.300
					277	−0.143		
CuHL	18.50(5)	6.35	minor					
CuL	12.15(5)	6.86	573	93	649	−0.030	200	2.208
					572	0.122		
					487	−0.230		
					322	0.789		
					260 (sh)	1.676		
$CuH_{-1}L$	4.24(3)	7.91	562	99	594	0.617	200	2.208
					484	0.608		
					322	1.534		
					288	4.010		
$CuH_{-2}L$	−5.42(3)	9.66	559	100	590	0.913	213	2.176
			517	100	483	−0.759		
					321	1.733		
					287	−0.429		
$CuH_{-3}L$	−15.87(3)	10.45	minor					

[a] Metal-to-ligand ratio = 1:1, $[Cu^{2+}]$ = 0.001 M.

and HSQC standard 2D sequences. Spectra processing was performed on a Silicon Graphics O2 workstation using the XWINNMR 2.6 software.

Spin lattice relaxation rates (R_1) were measured with inversion recovery (IR) pulse sequences. All rates were calculated by regression analysis of the initial recovery curves of longitudinal magnetization components leading to errors not larger than ±3%. Instead of the simple inversion recovery sequence, suitable for well-isolated signals, the IR−TOCSY sequence was applied to overlapping NMR resonances (*29*). The T_1 values were determined by a three-parameter fit of peak intensities to the following equation:

$$I(\tau) = I_0[1 - (1 + B)\exp(-\tau/T_1)]$$

B is a variable parameter (<1) which takes nonideal magnetization into account. The obtained results were compared with those obtained from a normal IR sequence. The agreement was found in the error limit of both experiments.

Structure Determination and MD Calculations. All R_{1p} values, obtained from NMR measurements (vide infra), were converted into distance constraints and used to build a pseudopotential energy for a restrained simulated annealing calculation in torsional angle space. In particular, we performed the calculation with the program DYANA (*30*), using 10 000 steps and 300 random relative starting positions of the peptide and Cu(II). Since only one molecule can be given as input in the program, the peptide was linked to Cu(II) through a long chain of linkers, i.e., residues made by atoms without van der Waals radius. These linkers could freely rotate around their bonds, without causing steric repulsions, and thus enable one to sample a large number of relative positions of the ligand with respect to the metal ion before the minimization step.

On the best structures of the investigated complexes obtained with this procedure we performed a restrained energy minimization followed by a restrained MD simulation in explicit water, using the program Hyperchem (*31*) with the Amber force field (*32*). Throughout the simulations we kept the experimentally derived metal−proton distance restraints already used for structure determination, and we additionally imposed the binding of copper(II) to its coordinating nitrogens. The coordinating amide nitrogens were deprotonated and the type of histidine (deprotonated at Nδ or Nϵ) was chosen in each case according to the experimental information on its binding mode. First, the structures were energy minimized in vacuo, then they were solvated using a parallelepiped box of water with periodic boundary conditions, with a minimum distance between solvent and solute atoms of 0.23 nm and each of the box dimensions set to twice the dimension of the complex along the corresponding axis. The resulting systems (complex + water) were again energy minimized and subsequently brought to the temperature of 288 K through three MD runs in which the temperature was progressively raised. Then an MD simulation of 14 ps at constant temperature (T = 288 K) was performed. Throughout the simulations, the time step was set to 1 fs and nonbonded interactions were treated using a twin range method, with an outer cutoff radius set to one-half of the smallest box dimension and an inner one set to 0.4 nm less.

RESULTS

Fugu1 or $StPrP_{96-104}$. Fugu1 exhibits four protonation constants with log K 6.77 and 6.04 assigned to two His imidazoles and 9.50 and 10.19 assigned to two phenolates of Tyr residues, respectively (Table 1). Potentiometric titrations of the Cu(II)/fugu1 solution are consistent with seven mononuclear species: CuH_3L, CuH_2L, CuHL, CuL,

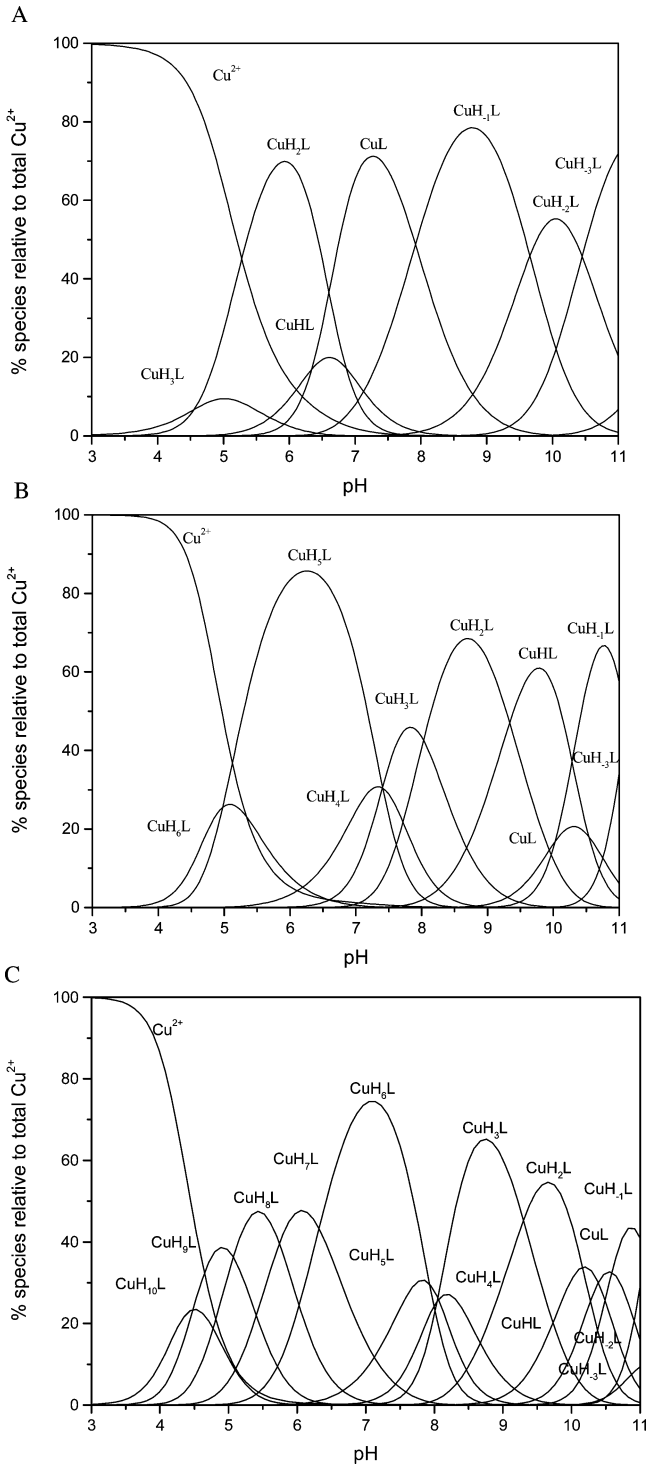

FIGURE 1: Species distribution profile for Cu^{2+} complexes of (A) fugu1 at 298 K and $I = 0.1$ M KNO_3, $[Cu^{2+}] = 1 \times 10^{-3}$ M, metal-to-ligand ratio of 1:1; (B) fugu2 at 298 K and $I = 0.1$ M KNO_3, $[Cu^{2+}] = 7 \times 10^{-4}$ M, metal-to-ligand ratio of 1:1; (C) fugu3 at 298 K and $I = 0.1$ M KNO_3, $[Cu^{2+}] = 7 \times 10^{-4}$ M, metal-to-ligand ratio of 1:1.

$CuH_{-1}L$, $CuH_{-2}L$, and $CuH_{-3}L$ (Figure 1A). The CuH_3L complex is a minor species with the Cu(II) ion anchored at imidazole nitrogen of one His residue. This species transforms to CuH_2L dominating in acidic pH. The value of log $K^* = \log \beta_{CuH2L} - \log \beta_{H2L} = 5.67$ agrees with coordination of Cu(II) ion by two imidazole nitrogens (*15*, *33*, *34*), as it is also supported by the d−d transition at 689 nm, the EPR parameters ($A_{||} = 170$ G; $g_{||} = 2.305$) (*35*), and by the appearance of the CD charge-transfer band at 279 nm (Table 1) (*36*). CuHL is a minor species and possibly corresponds to the $\{2N_{im}, N^-\}$ coordination mode. The CuL species, which dominates in the pH range of 7.0−8.0, involves the $\{2N_{im}, 2N^-\}$ donor set, as indicated by the EPR parameters ($A_{||} = 200$ G; $g_{||} = 2.208$), the d−d band which shifts to 573 nm (*35*), and also by the charge-transfer band at 322 nm (*36*). The deprotonation of CuL yields $CuH_{-1}L$ which dominates at pH ca. 9. The lack of the charge-transfer band between 390 and 415 nm strongly indicates that phenolate group of Tyr residue does not participate in the metal coordination (*34*, *37*). $CuH_{-2}L$ is successively formed through binding of a third amide nitrogen, as confirmed by the distinct changes in the spectroscopic parameters. Occurrence of a $\{N_{im}, 3N^-\}$ donor set is in fact consistent with the d−d band at 517 nm and by the change in EPR parameters ($A_{||} = 213$ G; $g_{||} = 2.176$). Deprotonation of the second Tyr residue leads to $CuH_{-3}L$, where the phenolate rings do not participate in coordinating the metal.

Table 2: Proton Paramagnetic Relaxation Contributions (R_{1p}), Copper−Proton Distances (r), and the Derived Exchange Time Values of 2 mM fugu1, pH 7.0, $T = 288$ K in 90% H_2O, 10% D_2O Calculated in the Presence of 0.02 Cu(II) Equiv

	R_{1p} (s^{-1})	r (nm)	τ_{M2} (ms)
Ac	0.54	0.79	
Gly-98 Hα	1.64	0.30−0.40	
Tyr-99 Hα	1.59	0.30−0.40	
Gly-100 Hα	1.15	0.61	
Val-101 Hα	1.04	0.64	
Val-101 Hβ	1.17	0.60	12
Val-101 Hγ	0.84	0.70	
Tyr-102 Hα	1.04	0.64	
Tyr-102 Hε	1.25	0.78	
Gly-103 Hα	1.40	0.53	

The ^1H and ^{13}C NMR assignments of fugu1 in water at pH 7 are reported in Tables 1s and 2s. To minimize exchange broadening of amide proton resonances, ^1H NMR experiments were performed at 288 K instead of the temperature (298 K) used for the ^{13}C NMR. Experiments were run at pH 7.0 and 9.0, where predominance of CuL and $CuH_{-1}L$, respectively, was shown by potentiometric titrations (vide supra).

Addition of Cu(II) at pH 7.0 caused selective proton and carbon line broadening (Figures 2A and 2s) that mainly affects aromatic His signals, thus suggesting contemporaneous involvement of His-97 and His-104 imidazole nitrogens in Cu(II) binding. Furthermore, the carbonyl signals of His-97, Gly-98, and His-104 (Figure 2B) were strongly broadened after the addition of 0.1 Cu(II) equiv indicating Gly-98 and Tyr-99 amide nitrogens as the additional donor atoms in CuL.

Proton relaxation rates were measured for the free peptide (R_{1f}) and in the presence of the metal ion (R_{1obs}). The obtained paramagnetic relaxation enhancements, $R_{1p} = R_{1obs} - p_f R_{1f}$, shown in Table 2, indicate that the region between the two His residues is the most affected. Besides all signals from His-97 and His-104 being so broadened that the corresponding relaxation rates could not be measured, the α-protons of Gly-98 and Tyr-99 were exhibiting the largest paramagnetic enhancements.

Addition of 0.5 Cu(II) equiv to the free peptide at pH 9.0 resulted in washing out of His aromatic signals in the ^{13}C 1D spectra (Figure 3A) and in a marked line broadening of

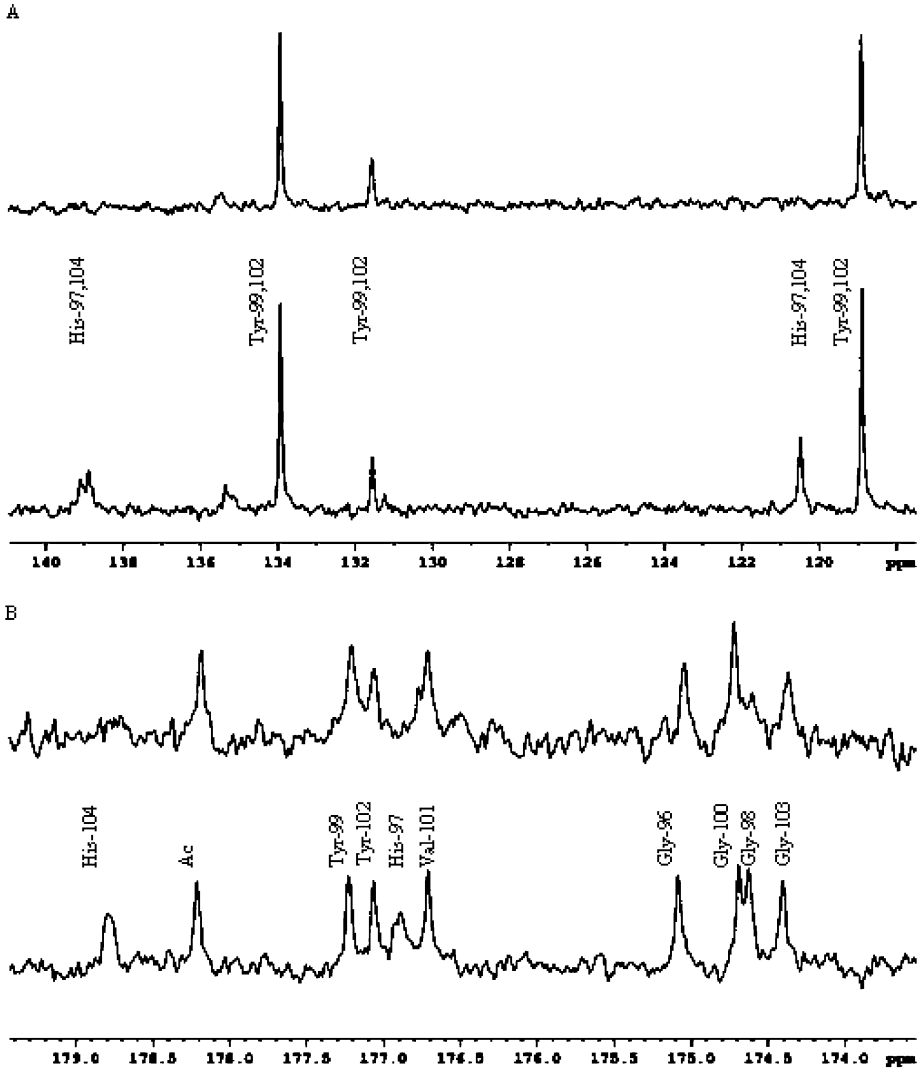

FIGURE 2: ^{13}C 1D spectrum of 5 mM fugu1 in D_2O at pH 7 and 298 K, free (lower trace) and in the presence of copper at 1:10 Cu(II)/peptide molar ratio (upper trace): (A) Aromatic region; (B) carbonyl region.

the majority of the carbonyl signals. In particular, those of His-97, Gly-98, Tyr-99, Gly-100, Val-101, Gly-103, and His-104 almost disappeared (Figure 3B). The effect of copper observed on His aromatic signals in the absence and in the presence of 0.1 Cu(II) equiv suggests the simultaneous involvement of the two His imidazole nitrogens in Cu(II) binding also in $CuH_{-1}L$.

Fugu2 or StPrP$_{96-116}$. Fugu2 behaves as an H_8L acid with protonation sites at the three imidazole nitrogens and at the five phenolic oxygens of the Tyr residues. The log *K* values of protonation constants of imidazole nitrogens vary from 5.5 to 6.8 and for the Tyr phenolic side chains from 9.4 to 11.3 in agreement with the literature data for similar peptides (Table 3) (*15*, *18*, *20*, *24*, *33*).

The calculations based on the potentiometric data of the Cu(II)−fugu2 system indicate the formation of nine species (Figure 1B). The first minor complex CuH_6L is a two-imidazole-bound complex. Deprotonation of CuH_6L yields a very stable three-imidazole-bound species that dominates in the pH range of 5.0−7.0. The $\log K^* = \log \beta_{CuH5L} - \log \beta_{H5L} = 6.86$ is characteristic for three bound imidazole nitrogens (*18*), as also supported by the EPR parameters ($A_{||} = 185$ G; $g_{||} = 2.264$) and by the d−d transition at 643 nm. The two other species, CuH_4L and CuH_3L, dominate at physiological pH. The blue-shift of the d−d band to 623 nm is revealing for amide nitrogen coordination such that CuH_4L apparently involves the $\{3N_{im}, N^-\}$ donor set. The deprotonation of CuH_4L yields CuH_3L, where the $\{2N_{im}, 2N^-\}$coordination mode is very likely to occur, as suggested by spectroscopic data (*15*). CuH_2L dominates in the pH range of 8.0−9.5. In this case, a third amide nitrogen is involved in binding and the $\{N_{im}, 3N^-\}$ donor set is confirmed by spectroscopic parameters (*33*). The calculated log *K* values for the successive deprotonation reactions ($CuH_2L \rightarrow CuHL \rightarrow CuL \rightarrow CuH_{-1}L \rightarrow CuH_{-3}L$) vary from 9.33 to 11.11, in good agreement with deprotonation of the noncoordinating Tyr residues.

The ^1H and ^{13}C NMR assignments of fugu2 in water at pH 6.0 and 288 K are reported in Tables 3s and 4s. Some sets of signals are partially or completely overlapped: Tyr-99 and Tyr-112 have completely overlapped signals, 5 of the 10 glycines, Gly-98, Gly-100, Gly-108, Gly-111, and Gly-113 display both Hα and HN resonances grouped in a very narrow ppm range, the His-97 and His-110 β-protons are overlapped in a way that prevents specific assignment of the corresponding aromatic protons.

Addition of Cu(II) selectively broadens proton lines, affecting all His signals. The connectivities of His aromatic

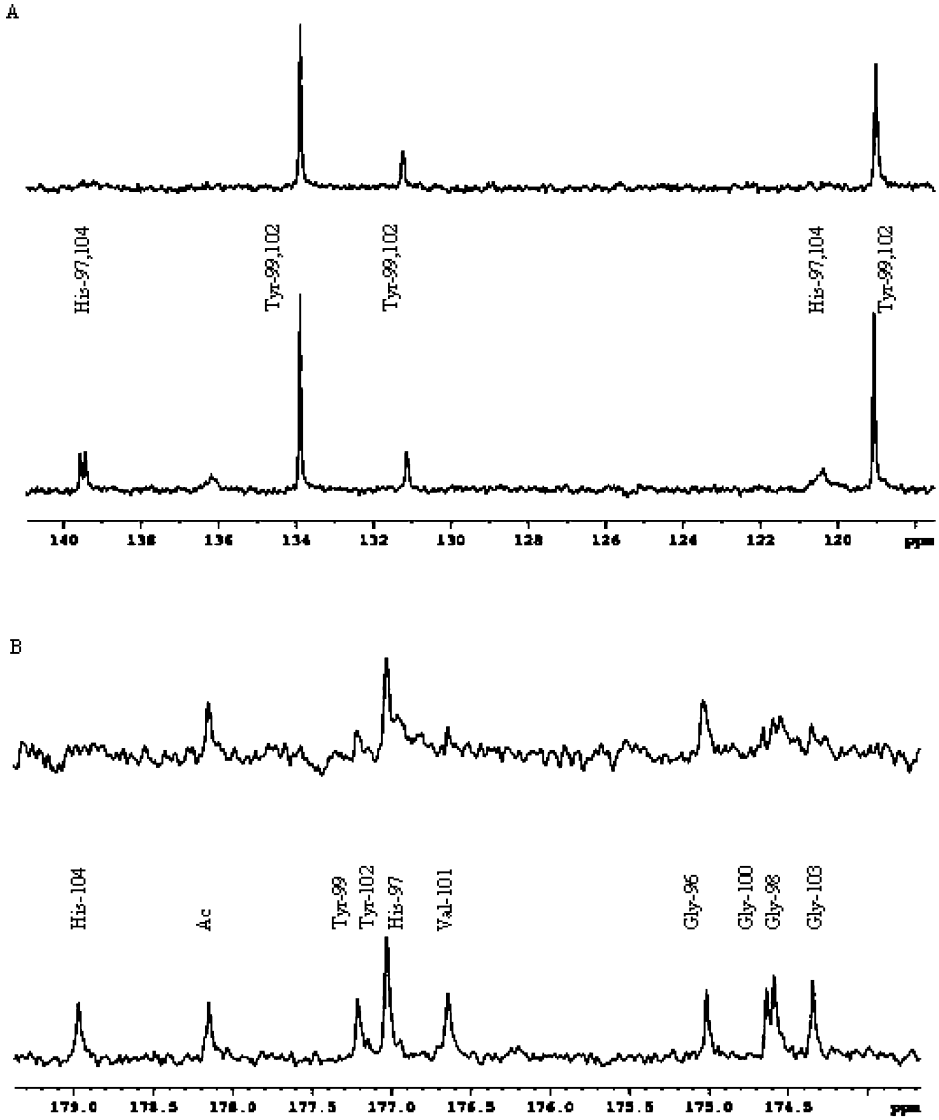

FIGURE 3: ^{13}C 1D spectrum of 5 mM fugu1 in D_2O at pH 9 and 298 K, free (lower trace) and in the presence of copper at 1:2 Cu(II)/peptide molar ratio (upper trace): (A) Aromatic region; (B) carbonyl region.

and β-protons in the HSQC spectra recorded at 1:50 Cu(II)/fugu2 disappear (Figure 4), thus supporting the involvement of the three His imidazoles in metal binding. The further broadening of Pro-105 correlations might be explained just by considering its high proximity to the preceding His-104.

In the same way as fugu1, R_{1p} measurements disclosed the most affected signals belonging to His moieties (Table 4) and to the residues immediately preceding or following the three histidines such as Gly-96, Gly-98, Gly-103, Pro-105, Gly-109, and Gly-111 (Table 5), which again verifies the exclusive involvement of the three His imidazole nitrogens in metal binding.

Fugu3 or StPrP$_{96-128}$. Fugu3 behaves as an $H_{12}L$ acid with protonation constants corresponding to six imidazole nitrogens of His residues and six phenolate oxygens of Tyr residues (Table 6). The calculation based on pH titrations of equimolar fugu3−Cu(II) solutions indicates the formation of a series of mononuclear species (Figure 1C). Due to a considerable overlapping of these species, the assignment of the spectroscopic data to particular complexes was difficult. The first five species, $CuH_{10}L$, CuH_9L, CuH_8L, CuH_7L, and CuH_6L, correspond to multi-imidazole complexes involving from two to possibly six His side chains, respectively. The log $K^* = \log \beta_{CuH6L} - \log \beta_{H6L} = 9.16$ may suggest more than four imidazole nitrogens involved in the coordination process (*34*). Additionally, the weak blue-shift from 618 to 588 nm suggests an out-of-plane coordination donor set. However, the similar pK values of deprotonation of fourth and fifth imidazole in free and metal-bound ligand may indicate a rather weak, if any, interaction of the fifth and sixth His residues with apical positions of the metal coordination sphere. Because of the lack of intensive d−d bands in CD spectra up to pH 8, the imidazole-only coordination is very likely, as the binding via amide nitrogens brings Cu(II) close to the asymmetric α-carbons making the CD d−d bands strong. The deprotonation of the CuH_6L species may lead to substitution of the imidazole donors by amide nitrogens and formation of the 4N coordination with $\{3N^-, N_{im}\}$ donor sets in the CuH_3L complex. The calculated log K values of the step-by-step deprotonation reaction $CuH_3L \rightarrow CuH_{-3}L$ are consistent with deprotonation of Tyr phenolic groups which do not participate in metal binding.

In NMR spectra of fugu3 in water at pH 6.0 and 288 K, the first two units are completely overlapped and the third

Table 3: Potentiometric and Spectroscopic Data for Proton and Cu^{2+} Complexes of Ac−GHGYGVYGHPGYGGHGYGVYG−NH_2 in DMSO/H_2O Mixed Solution[a]

			UV−vis		CD		EPR	
species	log β	log K	λ/nm	ϵ/M^{-1} cm^{-1}	λ/nm	$\Delta\epsilon$/M^{-1} cm^{-1}	$A_{\parallel}$/G	$g_{\parallel}$
fugu2								
HL	11.33(1)	log K_{Tyr} = 11.33						
H_2L	22.30(1)	log K_{Tyr} = 10.97						
H_3L	32.79(1)	log K_{Tyr} = 10.49						
H_4L	43.06(1)	log K_{Tyr} = 10.27						
H_5L	52.45(2)	log K_{Tyr} = 9.39						
H_6L	59.26(1)	log K_{im} = 6.81						
H_7L	65.54(1)	log K_{im} = 6.28						
H_8L	71.10(3)	log K_{im} = 5.56						
CuH_6L	64.28(2)		minor					
CuH_5L	59.31(4)	4.97	643	48	598	−0.065	185	2.264
					310	0.011		
					276	−0.433		
CuH_4L	51.90(5)	7.41	623	63	593	−0.052	186	2.252
					328	0.034		
					272	−0.349		
CuH_3L	44.49(6)	7.41	603	75	560	0.025	199	2.200
					485	−0.027		
					332	0.172		
					282	−0.853		
CuH_2L	36.46(6)	8.03	582 (sh)	93	573	0.037	217	2.171
			513	105	476	−0.197		
					330	0.450		
					298	−0.309		
					268	1.169		
CuHL	27.13(3)	9.33	582 (sh)	95	575	0.485	217	2.173
			510	117	475	−0.187		
					330	0.447		
					299	−0.426		
					272	1.400		
CuL	16.89(3)	10.24	minor					
$CuH_{-1}L$	6.56(3)	10.33	582 (sh)	96	570	0.436	217	2.168
			509	117	474	−0.184		
					330	0.352		
					298	−0.367		
					277	0.619		
$CuH_{-3}L$	−15.66(3)		minor					

[a] Metal-to-ligand ratio = 1:1, $[Cu^{2+}]$ = 0.0007 M.

one can be only partially assigned. As for the His residues, their δ-proton signals were overlapped with those of tyrosines, while four of the six ϵ-proton signals were separated, although it was not possible to assign them to the specific residues. On these latter signals, extensive line broadening (Figure 5) and relaxation rate enhancements were caused by Cu(II) addition, which suggests involvement of all the six His imidazoles present in the peptide sequence in metal coordination.

DISCUSSION

All reported experiments indicate that copper is bound by the His imidazole(s) in all investigated peptide sequences. As given evidence by potentiometric titrations that provide the stoichiometry and the profile of stabilities of formed complexes, the major species at physiological pH arise from a coordination pattern in which copper is first anchored by a number of imidazole nitrogens depending on the number of His residues and is then bound by consecutive amide nitrogens, finally forming the $\{N_{im}, 3N^-\}$ complex.

The paramagnetic ion shortens the longitudinal and transverse relaxation times of dipolarly or scalarly coupled nuclei, thus broadening all the resonances nearby. Measuring the paramagnetic relaxation enhancements (R_{1p}) therefore provides a means to calculate the Cu(II)−proton distances to be used in MD simulations leading to a three-dimensional picture of the structure.

The paramagnetic contributions R_{1p} are defined as (*38*, *39*):

$$R_{1p} = R_{1obs} - p_f R_{1f} = \frac{p_b}{R_{1b}^{-1} + \tau_M} \quad (1)$$

where $\tau_M = k_{off}^{-1}$ is the residence time of peptide molecules in the metal coordination sphere, p_f and p_b are the fraction of free and bound peptides, R_{1obs} and R_{1f} are the spin−lattice relaxation rates measured, respectively, after the addition of copper and in the metal-free solution, and R_{1b} is the rate of ligand nuclei in the metal coordination sphere.

Copper binding in histidine-containing peptides with the N_{im} and N^- donor set is a multistep process, where His imidazole provides the first anchoring site, with the consecutive binding sites depending on the peptide fragment (*33*, *40*−*42*). In fact, two different exchange times were measured for the Cu(II)−fugu1 complex, a shorter one (τ_{M1}) for the imidazole protons and a longer one (τ_{M2}) for all other protons.

In the Cu(II)−fugu1 complex the calculated R_{1p} values (18.6 s^{-1} at Cu(II)/fugu1 1:100) of the His Hϵ (Hϵ−Cu(II)

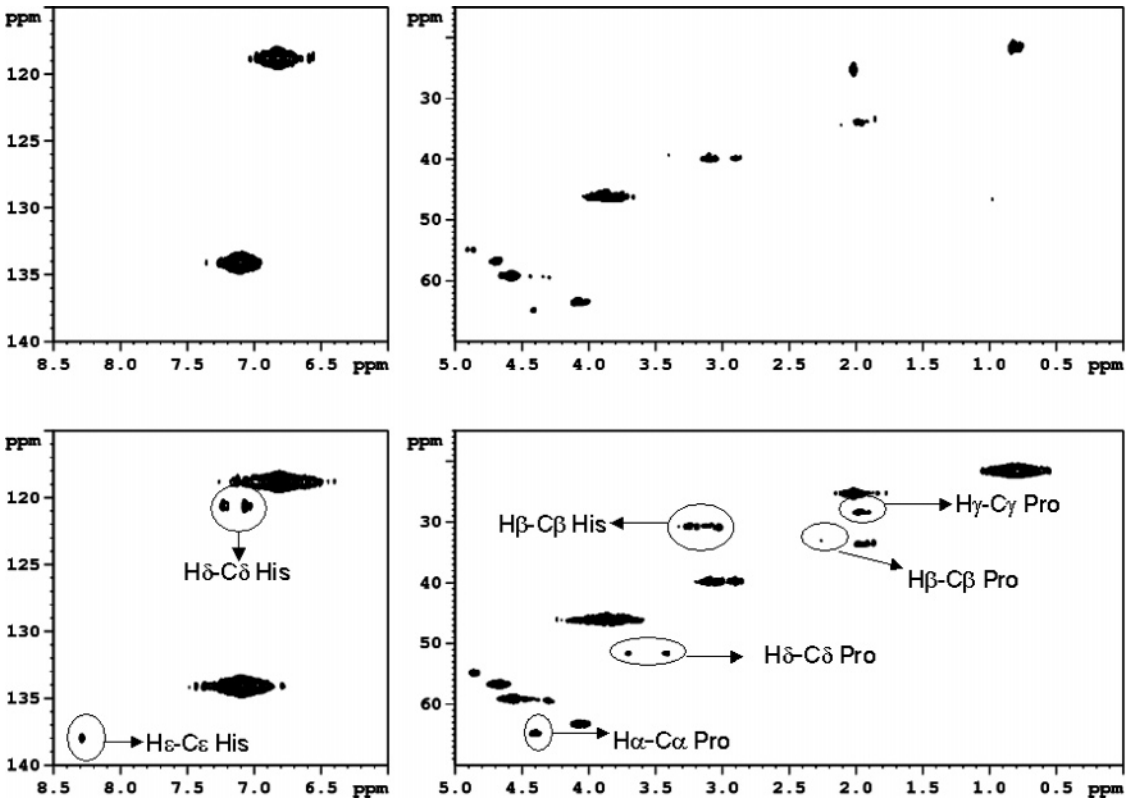

FIGURE 4: HSQC spectrum of 2 mM fugu2 in D_2O at pH 6 and 298 K, free (bottom) and in the presence of copper at 1:50 Cu(II)/peptide molar ratio (top).

Table 4: Proton Paramagnetic Relaxation Contributions (R_{1p}), Copper−Proton Distances (r), and the Derived Exchange Time Values of His Aromatic Protons for the Cu(II)−fugu2 Complex in 100% D_2O at pH 6, $T = 288$ K

				Hϵ			
Cu(II)	R_{1p} (s^{-1})				r (nm)		
equiv	His-97[a]	His-104	His-110[a]	τ_M (ms)	His-97	His-104	His-110
0.002	1.06	1.08	1.03	1.8			
0.004	2.23	2.25	2.22	1.7			
0.010	4.51	4.53	4.54	2.1			
0.020	10.09	10.12	10.16	1.9			
				Hδ			
0.002	0.98		0.84		0.37		0.42
0.004	1.93	1.71	1.76		0.38	0.42	0.42
0.010	3.90	3.30	3.74		0.40	0.45	0.42
0.020	9.26	8.32	8.66		0.37	0.41	0.40

[a] The two histidines are not unequivocally assigned.

distance 0.31 nm) allowed the determination of τ_{M1} at 0.5 ms, by using $\tau_c = 0.30 \pm 0.10$ ns, while the use of the Cu(II)−Gly-98 Hα distance ranging from 0.3 to 0.40 nm yielded $\tau_{M2} = 12$ ms.

The obtained τ_{M1} allowed us to ascertain which imidazole nitrogen, Nδ or Nϵ, is bound to the paramagnetic ion in the fugu1 complex, since the Cu(II)−His-Hδ distance depends on Cu(II) binding at Nδ ($r = 0.50$ nm) or at Nϵ ($r = 0.31$ nm) (*43*−*44*). The R_{1p} value (13.1 s^{-1} at Cu(II)/fugu1 1:100) calculated for the overlapping signals of the two His Hδ yielded a distance of 0.38 nm, suggesting that the two histidines diversely coordinate the copper ion, one via Nδ, the other via Nϵ. The His binding Cu(II) through Nϵ can be identified as His-104, since binding of Gly-98 and Tyr-99 creates such a steric hindrance that the His-97 Nϵ involvement can be excluded.

The metal−proton distances calculated using τ_{M2} (Table 2), together with additional distance restraints on the four coordinating nitrogens, allowed us to determine the structure of the Cu(II)−fugu1 complex through a restrained simulated annealing procedure (Figure 6A). On the obtained structure an energy minimization followed by an MD simulation were performed (Figure 6A). The backbone RMSD calculated on all the reported structures from residue 2 to residue 9 is 0.016 nm.

All these findings reveal that Cu(II), after anchoring at the two His imidazoles, deprotonates the amide nitrogens following His-97, toward the C-terminus. It is usually found that copper amide deprotonation takes place in the N-terminal direction which results in the formation of a more stable six-membered chelate ring. The involvement of amide nitrogens toward the C-terminal direction is likely to be stabilized by the simultaneous binding of both His imidazole rings which force the peptide to bend around the metal ion.

The fugu1 copper coordination sphere, however, is strictly dependent on the pH. CD and UV−vis parameters at pH > 7.0 indicate the formation of a diverse 4N complex in which a third amide nitrogen takes the place of one of the His imidazole nitrogens (Figure 3s). The substitution of imidazole nitrogens by amide nitrogen donors shifts the d−d transitions toward higher energies (Table 1). However, the copper-induced broadening of both His Cϵ resonances (Figure 3A) strongly supports that both His residues are bound. The paramagnetic contributions (R_{1p}= 20.4 s^{-1} at Cu(II)/fugu1 1:10) measured on His Hϵ at pH 9, allow the determination of the exchange time for the imidazole protons (vide supra), yielding a value of 4.8 ms. This value is about 10 times larger than those calculated at physiological pH (0.5 ms) strongly suggesting the rearrangement of the Cu(II) complex.

Table 5: Proton Paramagnetic Relaxation Contributions (R_{1p}) and Copper−Proton Distances (r) of 1 mM fugu2, pH 6.0, $T = 288$ K, in 90% H_2O, 10% D_2O Calculated in the Presence of 0.02 Cu(II) Equiv

	R_{1p} (s^{-1})	r (nm)		R_{1p} (s^{-1})	r (nm)
Ac	0.305	0.91			
Gly-96 Hα	1.16	0.72	Tyr-107 Hβ	0.79	0.77
Gly-98 Hα	1.41	0.69	Gly-108 Hα	0.67	0.795
Gly-100 Hα	0.20	0.98	Gly-109 Hα	0.92	0.75
Val-101 Hβ	0.40	0.87	Gly-111 Hα	1.41	0.69
Val-101 Hγ	0.39	0.87	Gly-113 Hα	0.20	0.98
Tyr-102 Hα	0.36	0.885	Val-114 Hα	0.165	1.01
Tyr-102 $H\beta_{1,2}$	0.61−0.50	0.81−0.84	Val-114 Hβ	0.14	1.04
Gly-103 Hα	1.21	0.71	Val-114 Hγ	0.45	0.85
Pro-105 Hα	0.45	0.85	Tyr-115 Hα	0.17	1.01
Pro-105 Hβ	0.20	0.98	Tyr-115 $H\beta_{1,2}$	0.44−0.21	0.86−0.97
Pro-105 Hδ	0.90	0.75	Gly-116 Hα	0.32	0.90
Gly-106 Hα	0.73	0.78	NH_2	0.22	0.96

Table 6: Potentiometric and Spectroscopic Data for Proton and Cu^{2+} Complexes of Ac−GHGYGVYGHPGYGGHGYGVYGHPGYGGHGFHGR−NH_2 DMSO/H_2O Mixed Solution[a]

			UV−vis		CD		EPR	
species	log β	log K	λ/nm	ε/M^{-1} cm^{-1}	λ/nm	Δε/M^{-1} cm^{-1}	$A_{\|\|}$/G	$g_{\|\|}$
fugu-3								
HL	11.51(1)	log $K_{Tyr} = 11.51$						
H_2L	22.45(1)	log $K_{Tyr} = 10.94$						
H_3L	33.39(1)	log $K_{Tyr} = 10.94$						
H_4L	43.72(1)	log $K_{Tyr} = 10.33$						
H_5L	53.94(2)	log $K_{Tyr} = 10.22$						
H_6L	63.28(1)	log $K_{Tyr} = 9.34$						
H_7L	70.33(1)	log $K_{im} = 7.05$						
H_8L	76.92(3)	log $K_{im} = 6.59$						
H_9L	83.20(2)	log $K_{im} = 6.28$						
$H_{10}L$	89.12(1)	log $K_{im} = 5.92$						
$H_{11}L$	94.75(1)	log $K_{im} = 5.63$						
$H_{12}L$	99.89(1)	log $K_{im} = 5.14$						
$CuH_{10}L$	94.05(3)		minor					
CuH_9L	89.57(4)	4.48	647	59	556 306 285	−0.075 0.053 −0.579	195	2.248
CuH_8L	84.50(5)	5.07	618	66	550 306 283	−0.127 0.092 −1.138	195	2.241
CuH_7L	78.76(6)	5.74	605	75	554 307 284	−0.150 0.115 −0.735	195	2.238
CuH_6L	72.44(6)	6.32	588	97	553 302 284	−0.142 0.130 −0.672	211	2.224
CuH_5L	64.51(6)	7.93	minor					
CuH_4L	56.45(7)	8.04	minor					
CuH_3L	48.41(7)	8.06	525 589 (sh)	127 112	607 485 335 300 283	0.510 −0.333 0.304 −0.954 1.114	211	2.170
CuH_2L	39.11(7)	9.30	517 589 (sh)	142 117	608 487 336 300	0.614 −0.453 0.269 −1.068	211	2.170
CuHL	28.95(6)	10.16	minor					
CuL	18.56(6)	10.39	minor					
$CuH_{-1}L$	7.97(5)	10.59	519 589 (sh)	139 112	604 484 339 304	0.554 −0.389 0.183 −1.038	211	2.166
$CuH_{-2}L$	−3.67(5)	11.64	minor					
$CuH_{-3}L$	−15.47(4)	11.80	minor					

[a] Metal-to-ligand ratio = 1:1, $[Cu^{2+}] = 0.0007$ M.

Moreover, the R_{1p} value ($R_{1p} = 15.7$ s^{-1} at a Cu(II)/fugu1 1:10) calculated for the overlapping signals of the two His Hδ yields a distance of 0.50 nm, which is very different from that obtained at pH 7 (0.38 nm) and indicates that the

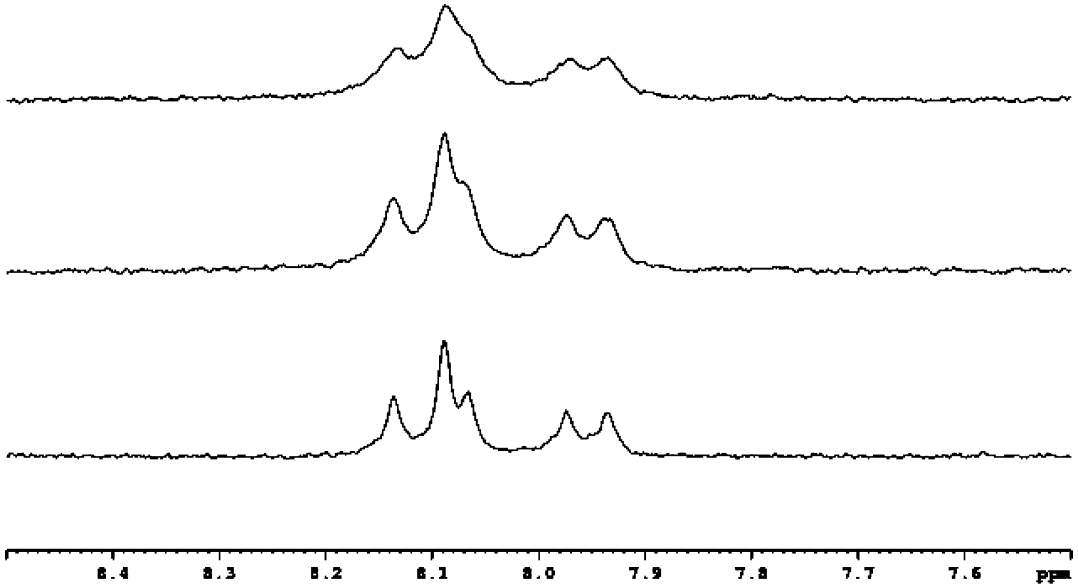

FIGURE 5: ^{1}H 1D spectrum of 1 mM fugu3 in D_2O at pH 6 and 288 K, free and in the presence of copper at 1:50 and 1:20 Cu(II)/peptide molar ratio (from bottom to top), showing only the region containing the His Hϵ signals.

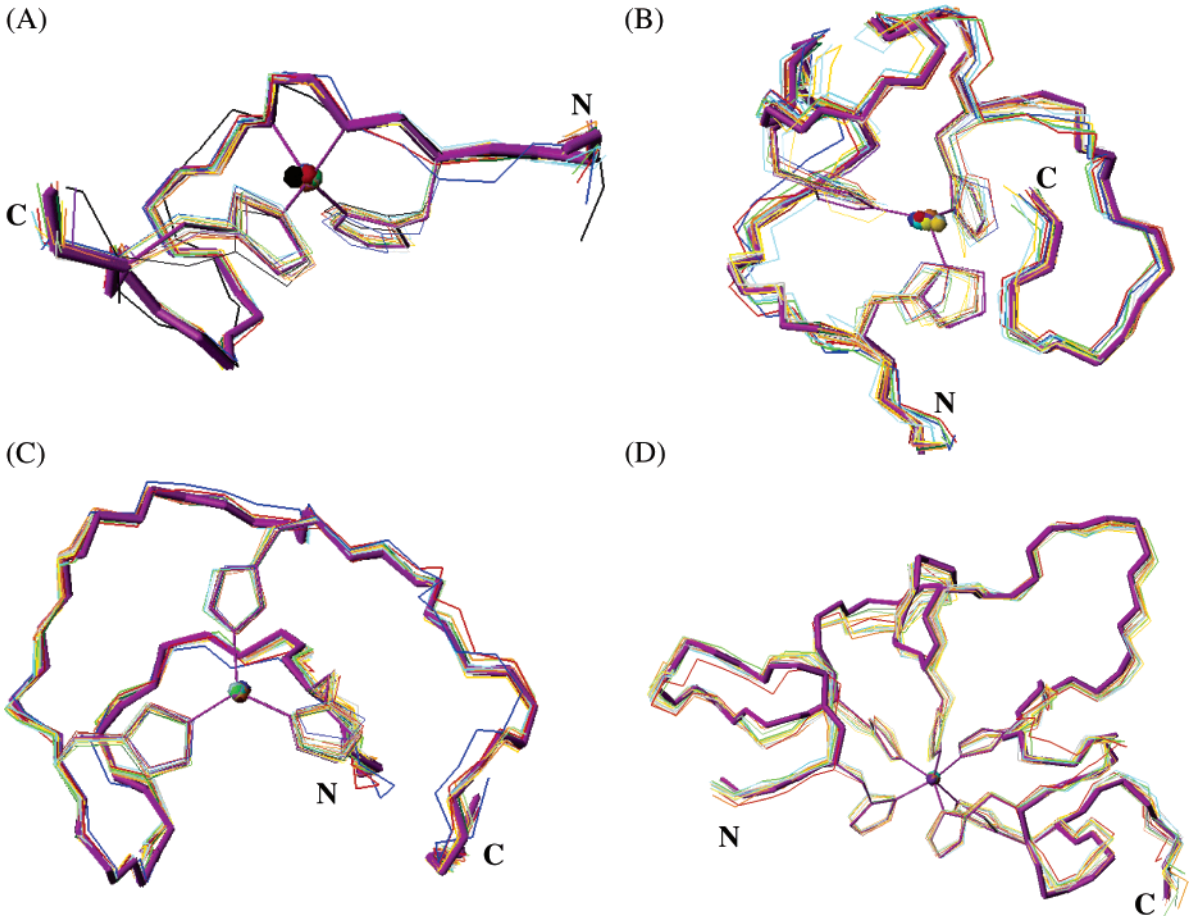

FIGURE 6: Structures of the Cu(II) complexes obtained through restrained simulated annealing and MD. Color codes are the following: black = structure from DYANA program, blue = minimized in vacuo, red = minimized in water, green = brought to 288 K, magenta = after 14 ps of MD at 288 K. All the other colored structures represent the snapshots from MD: (A) Cu(II)−fugu1; (B) Cu(II)−fugu2 with His-110 coordinating copper through its δ nitrogen; (C) Cu(II)−fugu2 with His-110 coordinating copper through its ϵ nitrogen; (D) Cu(II)−fugu3. The figure was created with MOLMOL 2K.1.0.

paramagnetic ion is bound to both His at Nδ. These findings, together with the extensive broadening of all ^{13}C NMR carbonyl signals (Figure 3B), can only be made consistent with the above-mentioned data from other spectroscopic techniques under the assumption of the coexistence of two Cu(II)−fugu1 complexes, one with the metal being coordi-

nated by His-97 imidazole Nδ and by the amide nitrogens of Gly-98, Tyr-99, and Gly-100, the other with copper coordination involving His-104 Nδ and the amide nitrogens of His-104, Gly-103, and Tyr-102.

The paramagnetic contributions measured for the Cu(II)−fugu2 complex were measured, and as in the case of the monomeric unit, a set of copper−proton distances were obtained. In this case a single exchange time was obtained, since metal binding occurs only at imidazole nitrogens, and its value was calculated using the Hϵ(His)−Cu(II) fixed distance, and a τ_c of 0.60 ± 0.10 ns, resulting into a value of 1.9 ms (Table 4). This τ_M was used to calculate the metal−proton distances for the Cu(II)−fugu2 complex (Tables 4 and 5). The obtained averaged Hδ(His)−Cu(II) distances of 0.38 nm for His-97, 0.43 nm for His-104, and 0.415 nm for His-110 are intermediate between the values corresponding to metal binding to Nδ or to Nϵ. This indicates the occurrence of an equilibrium among several complexes with the two possible metal coordination modes for each of the three histidines. To allow a comparison with the Cu(II)−fugu1 complex at pH 7.0, the two conformers obtained maintaining for His-97 and His-104 a coordination mode similar to that observed in fugu1 unit were considered, with His-97 binding copper through Nδ and His-104 through Nϵ, and allowing for His-110 both possible binding modes.

The structures of the Cu(II)−fugu2 complex were obtained through restrained simulated annealing based on the metal−proton distances in Table 5. On the two obtained conformations, an energy minimization followed by an MD simulation were performed (Figure 6B and C). The backbone RMSD calculated on all the reported structures from residue 97 to residue 110 is 0.033 and 0.040 nm for the conformation with His-110 binding through Nδ or to Nϵ, respectively.

Also in the case of Cu(II)−fugu3 complex the exchange time τ_M was calculated from the Hϵ(His) R_{1p} values (ranging from 7.27 to 7.88 s^{-1}) by using the Hϵ−Cu(II) fixed distance and a τ_c of 0.90 ± 0.10 ns, resulting into an averaged value of 6.5 ms at 288 K.

The above-mentioned extensive overlap of resonances, and the consequent lack of a sequential assignment, prevented the calculation of metal−proton distances from relaxation rate enhancements and their use as restraints for structure determination of the Cu(II)−fugu3 complex. Moreover, due to the overlap of His Hδ signals with those of tyrosines, no information on the binding mode (through Nδ or Nϵ) of each histidine could be achieved.

To model the effect of metal binding on the peptide global conformation, we performed an MD simulation of the complex starting from an extended structure of the fugu3 peptide and imposing only copper coordination to all six histidines, considering a metal binding mode for the imidazoles of each repeat analogous to that observed for the monomeric unit (Figure 6D). The RMSD calculated on the His residues of all the reported structures is 0.033 nm.

All the investigated peptides, derived from the tandem region of the fugu prion protein PrP2, behave as strong copper chelators at pH > 6. The obtained findings suggest the involvement of all or most of the His residues in copper coordination. As observed for human and chicken prion protein, copper binding in the tandem repeat region is characterized by multi-imidazole coordination at pH < 7, while the involvement of amide nitrogens is observed at physiological pH. Since the evaluated exchange times of the anchoring site are directly related to K_d, a comparison of the τ_M values suggests that the three considered fragments bind copper with affinities in the order fugu 3 > fugu2 > fugu1 (Figure 4s).

The multi-imidazole coordination pattern is characteristic for all tandem repeats in mammalian, avian, and fugu proteins and it is a favored binding mode for low Cu(II) concentrations. Higher metal ion concentrations and higher pH favor the involvement of amide nitrogen donors in the Cu(II) coordination. In the case of mammalian PrP^C the Pro residue inserted in front of His residue in octarepeat unit (PHGGGWGQ) forces the involvement of amides of GGG fragment (*15*, *33*). In the case of avian protein the presence of two Pro residues in the hexapeptide sequence (PHNPGY) changes the binding ability of amide donors completely. The amide nitrogen of Pro inserted into the peptide sequence does not bind Cu(II) ion, and the metal ion coordination is limited to imidazole and one peptide bond amide (*18*, *34*, *42*). In the case of fugu protein Pro is inserted only in the linker region, and the impact of this residue on the binding ability of repeat region is a minor factor and the amount of amide nitrogens involved in the Cu(II) binding is similar to that found in mammalian peptide. The comparison of the binding ability of fugu and human peptide unit (fugu1 and PHGGGWGQ) clearly shows that the fugu fragment is much more effective in Cu(II) ion binding (Figure 5s). The same could be found in the case of whole human repeat region and fugu3 representing repeat region of fugu protein (Figure 6s).

SUPPORTING INFORMATION AVAILABLE

^{1}H chemical shift assignment (ppm) of the monomeric unit of *Takifugu rubripes* prion protein in water at pH 7 and 288 K (Table 1s); ^{13}C chemical shift assignment (ppm) of the monomeric unit of *T. rubripes* prion protein in water at pH 7 and 298 K (Table 2s); ^{1}H chemical shift assignment (ppm) of the dimeric unit of *T. rubripes* prion protein in water at pH 6 and 288 K (Table 3s); ^{13}C chemical shift assignment (ppm) of the dimeric unit of *T. rubripes* prion protein in water at pH 6 and 298 K (Table 4s); MALDI-TOF MS spectra of the monomeric, dimeric, and trimeric units of *T. rubripes* prion protein (Figure 1s); ^{1}H 1D spectrum of the monomeric unit of *T. rubripes* prion protein in water at pH 7 and 288 K, free and in the presence of copper at 1:100, 1:50, and 1:10 Cu(II)/peptide molar ratios (from bottom to top) (Figure 2s); CD (A) and UV−vis (B) spectra of two different 4N complexes of fugu1/CuL $\{2N_{im}, 2N^-\}$ and $CuH_{-1}L$ $\{1N_{im}, 3N^-\}$ (Figure 3s); distribution profiles of competition between fugu1 and fugu3 in coordination of one Cu^{2+}, $[Cu^{2+}] = 5 \times 10^{-4}$ M, ligand (fugu1) to metal to ligand (fugu3) ratio of 1:1:1 (Figure 4s); distribution profiles of competition between fugu1 and human octarepeated unit (PHGGGWGQ) in coordination of one Cu^{2+}, $[Cu^{2+}] = 1 \times 10^{-3}$ M, ligand (fugu1) to metal to ligand (PHGGGWGQ) ratio of 1:1:1 (Figure 5s); distribution profiles of competition between fugu3 and human octarepeated domain $(PHGGGWGQ)_4$ in coordination of one Cu^{2+}, $[Cu^{2+}] = 5 \times 10^{-4}$ M, ligand (fugu3) to metal to ligand $(PHGGGWGQ)_4$ ratio of 1:1:1 (Figure 6s). This material is available free of charge via the Internet at http://pubs.acs.org.

REFERENCES

1. Prusiner, S. B. (1998) Prions, *Proc. Natl. Acad. Sci. U.S.A. 95*, 13363−13383.
2. Brown, D. R., Wong, B. S., Hafiz, F., Clive, C., Haswell, S. J., and Jones, I. M. (1999) Normal prion protein has an activity like that of superoxide dismutase, *Biochem. J. 344*, 1−5.
3. Billeter, M., Riek, R., Wider, G., Hornemann, S., Glockshuber, R., and Wüthrich, K. (1997) Prion protein NMR structure and species barrier for prion diseases, *Proc. Natl. Acad. Sci. U.S.A. 94*, 7281−7285.
4. Kocisko, D. A., Priola, S. A., Raymond, G. J., Chesebro, B., Lansbury, P. T., Jr., and Caughey, B. (1995) Species specificity in the cell-free conversion of prion protein to protease-resistant forms: a model for the scrapie species barrier, *Proc. Natl. Acad. Sci. U.S.A. 92*, 3923−3927.
5. Telling, G. C., Scott, M., Hsiao, K. K., Foster, D., Yang, S., Torchia, M., Sidle, K. C. L., Collinge, J., DeArmond, S. J., and Prusiner, S. B. (1994) Transmission of Creutzfeldt-Jakob disease from humans to transgenic mice expressing chimeric human−mouse prion protein, *Proc. Natl. Acad. Sci. U.S.A. 91*, 9936−9940.
6. Horiuchi, M., Priola, S. A., Chabry, J., and Caughey, B. (2000) Interaction between heterologous forms of prion protein: binding, inhibition of conversion, and species barrier, *Proc. Natl. Acad. Sci. U.S.A. 97*, 5836−5841.
7. Lysek, D. A., Schorn, C., Nivon, L. G., Esteve-Moya, V., Christen B., Calzolai, L., Von Schroetter, C., Fiorito, F., Herrmann, T., Guntert, P., and Wuthrich, K. (2005) Prion protein NMR structures of cats, dogs, pigs and sheep, *Proc. Natl. Acad. Sci. U.S.A. 102*, 640−645.
8. Calzolai, L., Lysek, D. A., Perez, D. R., Guntert, P., and Wuthrich, K. (2005) Prion protein NMR structures of chickens, turtles and frogs, *Proc. Natl. Acad. Sci. U.S.A. 102*, 651−655.
9. Gossert, A. D., Bonjour, S., Lysek, D. A., Fiorito, F., and Wuthrich, K. (2005) Prion protein NMR structures of elk and mouse/elk hybrids, *Proc. Natl. Acad. Sci. U.S.A. 102*, 646−650.
10. Zahn, R., Liu, A., Luhrs, T., Riek, R., von Schroetter, C., Lopez Garcia, F., Billeter, M., Calzolai, L., Wider, G., and Wuthrich, K. (2000) NMR solution structure of the human prion protein, *Proc. Natl. Acad. Sci. U.S.A. 97*, 145−150.
11. Rivera-Milla, E., Stuermer C. A. O., and Malaga-Trillo, E. (2003) An evolutionary basis for scrapie disease: identification of a fish prion mRNA, *Trends Genet. 19*, 72−75.
12. Oidtmann, B., Simon, D., Holtkamp, N., Hoffmann, R., and Baier, M. (2003) Identification of cDNAs from Japanese pufferfish (*Fugu rubripes*) and Atlantic salmon (*Salmo salar*) coding for homologues to tetrapod prion proteins, *FEBS Lett. 538*, 96−100.
13. Gabriel, J. M., Oesch, B., Kretzschmar, H., Scott, M., and Prusiner, S. B. (1992) Molecular cloning of a candidate chicken prion protein, *Proc. Natl. Acad. Sci. U.S.A. 89*, 9097−9101.
14. Wopfner, F., Weidenhofer, G., Schneider, R., von Brunn, A., Gilch, S., Schwartz, T. F., Werner, T., and Schatzl, H. M. (1999) Analysis of 27 mammalian and 9 avian PrPs reveals high conservation of flexible region of the prion protein, *J. Mol. Biol. 289*, 1163−1178.
15. Valensin, D., Luczkowski, M., Mancini, F. M., Legowska, A., Gaggelli, E., Valensin, G., Rolka K., and Kozłowski, H. (2004) The dimeric and tetrameric octarepeat fragments of prion protein behave differently to its monomeric unit, *Dalton Trans*. 1284−1293.
16. Chattopadhyay, M., Walter, E. D., Newell, D. J., Jackson, P. J., Aronoff-Spencer, E., Peisach, J., Gerfen, G. J., Bennett, B., Antholine, W. E., and Millhauser, G. L. (2005) The octarepeat domain of the prion protein binds Cu(II) with three distinct coordination modes at pH 7.4, *J. Am. Chem. Soc. 127*, 12647−12656.
17. Garnett, A. P., and Viles, J. H. (2003) Copper binding to the octarepeats of the prion protein. Affinity, specificity, folding and cooperativity: insights from circular dichroism, *J. Biol. Chem. 278*, 6795−6802.
18. Stañczak, P., Valensin, D., Juszczyk, P., Grzonka, Z., Molteni, E., Valensin, G., Gaggelli, E., and Kozłowski, H. (2005) Structure and stability of the CuII complexes with tandem repeats of the chicken prion, *Biochemistry 44*, 12940−12954.
19. Redecke, L., Meyer-Klaucke, W., Koker, M., Clos, J., Georgieva, D., Genov, N., Echner, H., Kalbacher, H., Perbandt, M., Bredehorst, R., Voelter, W., and Betzel C. (2005) Comparative analysis of the human and chicken prion protein copper binding regions at pH 6.5, *J. Biol. Chem. 280*, 13987−13992.
20. La Mendola, D., Bonomo, R. P., Impellizzeri, G., Maccarrone, G., Pappalardo, G., Pietropaolo, A., Rizzarelli, E., and Zito, V. (2005) Copper(II) complexes with chicken prion repeats: influence of proline and tyrosine residues on the coordination features, *J. Biol. Inorg. Chem. 10*, 463−475.
21. Steward, J. M., and Young, J. D. (1993) *Solid-Phase Peptide Synthesis*, 2nd ed., Pierce Chemical Company, Rockford, IL.
22. *The Millipore 9050 Plus PepSynthesizer Operator's Guide* (1992) Millipore Corporation, Milford, MA.
23. Sole, N., and Barany, G. (1992) Optimization of solid-phase synthesis of [Ala8]-dynorphin A, *J. Org. Chem. 57*, 5399−5403.
24. Gran, G. (1950) Determination of the equivalent point in potentiometric titrations, *Acta Chem. Scand. 4*, 559−577.
25. Bataille, M., Formicka-Kozłowska, G., Kozłowski, H., Pettit, L. D., and Steel, I. (1984) The L-proline residue as a break-point in the coordination of metal−peptide systems, *J. Chem. Soc., Chem. Commun. 4*, 231−232.
26. Gans, P., Sabatini, A., and Vacca, A. (1985) SUPERQUAD: an improved general program for computation of formation constants from potentiometric data, *J. Chem. Soc., Dalton Trans*. 1195−1200.
27. Gans, P., Sabatini, A., and Vacca, A. (1996) Investigation of equilibria in solution. Determination of equilibrium constants with the HYPERQUAD suite of programs, *Talanta 43*, 1739−1753.
28. Hwang, T. L., and Shaka, A. J. J. (1995) Water suppression that works: excitation sculpting using arbitrary waveforms and pulse field gradients, *J. Magn. Reson., Ser. A 112*, 275−279.
29. Huber, J. G., Moulis, J. M., and Gaillard, J. (1996) Use of ^{1}H longitudinal relaxation times in the solution structure of paramagnetic proteins. Application to [4Fe−4S] proteins, *Biochemistry 35*, 12705−12711.
30. Güntert, P., Mumenthaler, C., and Wüthrich, K. (1997) Torsion angle dynamics for NMR structure calculation with the program DYANA, *J. Mol. Biol. 273*, 283−298.
31. HYPERCHEM (1997) Hypercube, Release 5.1 Pro for Windows, Hypercube Inc., Waterloo, ON.
32. Ponder, J. W., and Case, D. A. (2003) Force fields for protein simulations, *Adv. Protein Chem. 66*, 27−85.
33. Luczkowski M., Kozlowski H., Slawikowski M., Rolka K., Gaggelli E., Valensin D., and Valensin G. (2002) Is the monomeric prion octapeptide repeat PHGGGWGQ a specific ligand for Cu^{2+} ions? *J. Chem. Soc., Dalton Trans.* 2269−2274.
34. Stanczak, P., Luczkowski, M., Juszczyk, P., Grzonka, Z., and Kozłowski, H. (2004) Interactions of Cu^{2+} ions with chicken prion tandem repeats, *Dalton Trans*. 2102−2107.
35. Pettit, L. D., Gregor, J. E., and Kozlowski, H. (1991) in *Perspectives on Bioinorganic Chemistry* (Hay, R. W., Dilworth, J. R., and Nolan, K. B., Eds.) Vol. 1, pp 1−44, JAI Press, London.
36. Bal, W., Jezowska-Bojczuk, M., Kozłowski, H., Chruscinski, L., Kupryszewski, G., and Witczak, B. (1995) Cu(II) binding by angiotensin II fragments: Asp-Arg-Val-Tyr-Ile-His and Arg-Val-Tyr-Ile-His. Competition between amino group and imidazole nitrogens in anchoring of metal ions, *J. Inorg. Biochem. 57*, 235−247.
37. Pettit, L. D., Steel, I., Kowalik, T., Kozlowski, H., and Bataille, M. (1985) Specific binding of the tyrosine residue in copper(II) complexes of Tyr-Pro-Gly-Tyr and Tyr-Gly-Pro-Tyr, *J. Chem. Soc., Dalton Trans*. 1201−1205.
38. Bertini, I., and Luchinat, C. (1996) NMR of paramagnetic substances, *Coord. Chem. Rev. 150*, 1−294.
39. Solomon, I. (1955) Relaxation processes in a system of two spins, *Phys. Rev. 99*, 559−565.
40. Belosi, B., Gaggelli, E., Guerrini, R., Kozłowski, H., Łuczkowski, M., Mancini, F. M., Remelli, M., Valensin, D., and Valensin, G. (2004) Copper binding to the neurotoxic peptide PrP106-126: thermodynamic and structural studies, *ChemBioChem 5*, 349−359.
41. Gaggelli, E., Bernardi, F., Molteni, E., Pogni, R., Valensin, D., Valensin, G., Remelli, M., Luczkowski, M., and Kozlowski, H. (2005) Interaction of the human prion PrP(106−126) sequence with copper(II), manganese(II), and zinc(II): NMR and EPR studies, *J. Am. Chem. Soc. 127*, 996−1006.
42. Stañczak, P., Valensin, D., Juszczyk, P., Grzonka, Z., Valensin, G., Bernardi, F., Molteni, E., Gaggelli, E., and Kozlowski, H.

(2005) Fine-tuning the structure of the Cu(II) complex with the prion protein chicken repeat by proline isomerization, *Chem. Commun. 26*, 3298−3300.
43. Gaggelli, E., Kozłowski, H., Valensin, D., and Valensin, G. (2005) NMR studies on Cu(II)-peptide complexes: exchange kinetics and determination of structures in solution, *Mol. Biosyst. 1*, 79−84.
44. Gaggelli, E., D'Amelio, N., Valensin, D., and Valensin, G. (2003) ^{1}H NMR studies of copper binding by histidine-containing peptides, *Magn. Reson. Chem. 41*, 877−883.

BI061123K